Massive isotopic effect in vacuum UV photodissociation of N_2 and implications for meteorite data

Subrata Chakraborty[a,1], B. H. Muskatel[b], Teresa L. Jackson[a], Musahid Ahmed[c], R. D. Levine[b,d], and Mark H. Thiemens[a]

[a]Department of Chemistry and Biochemistry, University of California, San Diego, La Jolla, CA 92093-0356; [b]The Fritz Haber Research Center for Molecular Dynamics, The Hebrew University of Jerusalem, Jerusalem 91904, Israel; [c]Chemical Sciences Division, Lawrence Berkeley National Laboratory, Berkeley, CA 94720; and [d]Department of Chemistry and Biochemistry, Crump Institute for Molecular Imaging, and Department of Molecular and Medical Pharmacology, University of California, Los Angeles, CA 90095

Nitrogen isotopic distributions in the solar system extend across an enormous range, from −400‰, in the solar wind and Jovian atmosphere, to about 5,000‰ in organic matter in carbonaceous chondrites. Distributions such as these require complex processing of nitrogen reservoirs and extraordinary isotope effects. While theoretical models invoke ion-neutral exchange reactions outside the protoplanetary disk and photochemical self-shielding on the disk surface to explain the variations, there are no experiments to substantiate these models. Experimental results of N_2 photolysis at vacuum UV wavelengths in the presence of hydrogen are presented here, which show a wide range of enriched $\delta^{15}N$ values from 648‰ to 13,412‰ in product NH_3, depending upon photodissociation wavelength. The measured enrichment range in photodissociation of N_2, plausibly explains the range of $\delta^{15}N$ in extraterrestrial materials. This study suggests the importance of photochemical processing of the nitrogen reservoirs within the solar nebula.

nitrogen isotopes | organic molecules | perturbation

Nitrogen isotopic analyses of meteorites, terrestrial planets, atmospheres of giant planets and their moons, solar wind, comets, and interplanetary dust particles (1) may advance understanding of volatile chemistry and prebiotic processes in the early solar system.

Nitrogen Isotopic Compositions in Solar System

Nitrogen isotopic distributions, measured as $\delta^{15}N$ (with respect to air-N_2, where $\delta^{15}N = ((^{15}N/^{14}N)_{sample}/(^{15}N/^{14}N)_{air} - 1) \times 1,000‰$), in the solar system extend across an enormous range, from −400‰, in the solar wind (2) and Jovian atmosphere (3), to about 5,000‰ in organic matter in carbonaceous chondrites (4, 5).

Nitrogen Isotopic Composition Measured in Meteorites

Bulk meteorite analysis exhibits a variation in the range of a few hundred permil in $\delta^{15}N$ (6–8), with occasional exceptionally high values (Fig. 1A) found in two carbonaceous chondrites (i.e., Renazzo, $\delta^{15}N = -190‰$ to +150‰, and Isheyevo, $\delta^{15}N \approx 1,100‰$) (9, 10), two stony-iron meteorites (i.e., Bencubbin and Weatherford, where $\delta^{15}N \approx 973‰$) (11), and a few stony and iron meteorites (6, 12). The N-isotopic composition measured in a returned solar wind sample from the Genesis discovery mission and in the atmosphere of Jupiter (measured in NH_3) are nearly equally depleted (−400‰, Fig. 1A) (2, 3). Conversely, extremely high ^{15}N enrichments are observed (Fig. 1B) with high spatial resolution instruments (e.g., nano-secondary ion mass spectrometer) in meteoritic "hotspots" (regions of extreme ^{15}N enrichment, occasionally as high as ~5,000‰), interplanetary dust particles, cometary samples (including that from Stardust mission), and insoluble organic matter (IOM) from meteorites (4, 5, 13–15).

Isotopic Relationship Between N, C, and H in Extraterrestrial Reservoirs

The relationship of nitrogen isotopes with those of carbon and hydrogen is important because of their mutual presence in nitrile (-CN) and amine (-NH_2) functional groups in organic molecules. High ^{15}N enrichments are not correlated with carbon isotopes (e.g., $^{13}C/^{12}C$) (6–8, 16, 17), although there are occasional correlations with high D/H ratios (18). The D/H enrichment in the interstellar medium has been modeled at low temperatures (25 K), including ion-neutral exchange reactions (19). Models of ion−molecule exchange reactions at extremely cold temperatures for N isotopes include formation of ^{15}N-enriched functional groups in interstellar clouds. It is possible to form amine group molecules with ^{15}N enrichments of ~3,000‰ in this process (20, 21). Model uncertainties reside in the unknown rate coefficients of key exchange reactions (20). Ion-neutral exchange reaction models predict simultaneous D and ^{15}N enrichments. The lack of significant correlation between the two isotopic systems in the solar system weakens the premise that D and ^{15}N enrichments are of presolar origin (18). A recent model predicts uncorrelated D and ^{15}N enrichments and includes ortho and para forms of hydrogen in an ion−molecular reaction network (22) with uncertainties due to unknown rate coefficients of isotope exchange reactions. Processing of nitrogen through isotopologue selective photodissociation (i.e., isotope self-shielding) in the vacuum UV (VUV) wavelengths has been proposed (23) although there have been no experimental measurements.

Significance

In this paper, we account for the wide range (approximately a few thousand permil) of nitrogen isotopic composition measured in solar system materials. Several theoretical models have been proposed to explain the nitrogen isotopic enrichments measured in meteorites (especially in organic matter) and in cometary ice (NH_3 and/or HCN). These models include ion−molecular isotope exchange reactions and isotope self-shielding in the disk. However, a major limit is that there are no experiments to substantiate any model. We measured and found massive N-isotopic fractionations during vacuum UV photodissociation of N_2, perhaps one of the largest isotope effects ever measured, and present mechanistic evidence for the wide distribution in nitrogen isotopic compositions.
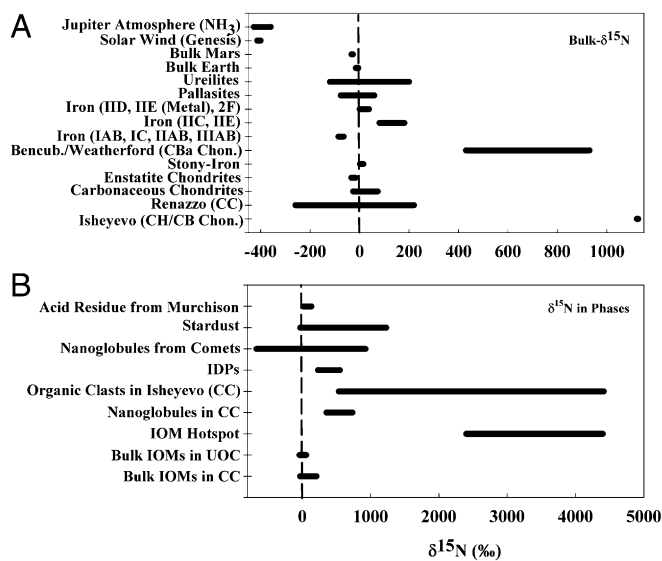
Fig. 1. Compiled nitrogen isotopic composition measured in meteorites and other solar system objects. (A) Bulk N-isotopic composition in meteorites, solar wind, and Jupiter. (B) N-isotopic compositions measured in different organic phases in meteorites and comets. The references used for compiling A and B are refs. 2, 3, 5, 6, 9–13, and 46–50.

Experimental Approach and Results

Photodissociation of a mixture of N_2 and H_2 was undertaken at different VUV wavelengths using the Advanced Light Source (ALS) synchrotron at the Lawrence Berkeley National Laboratory in a differentially pumped flow chamber. Five sets of experiments (described in Table 1) were performed, where in set-I, the N-isotopic compositions of the products (NH_3) of nine different photolysis (synchrotron wavelengths) experiments at a particular temperature (−78 °C) and gas-mixture pressure (100 mtorr) were measured. The results show (Table 1 and Fig. 2) large ^{15}N enrichments (of about a few thousand permil) in the wavelength span of 80–98 nm, and depict a peak at 90 nm (111,111 cm^{-1}), where an unprecedented ^{15}N enrichment of 11,780‰ (average of two separate experiments) is observed. It was previously calculated (24, 25) that an isotope effect in N_2 could result from extensive state mixing in localized spectral regions. To observe other state mixing dynamics, four other sets (set-II through set-V, Table 1) of experiments were performed with varying pressure and temperature. The ^{15}N enrichment profiles for these four sets of experiments also show large enrichments. The results from set-II experiments, which are at the same column densities as that of set-I (but at different temperatures), also show a peak at 90 nm, similar to that of set-I, although the peak enrichments are lower than that for set-I (Fig. 2). The measured ^{15}N enrichment values results from set-III experiments (at a different column density from set-I and set-II) are, within the error, identical to each other for wavelengths around 90 nm. The enrichments measured at 90 nm for set-IV and set-V experiments (performed at the same column densities as those of set-I and set-II) also show unusually high values similar to those measured in set-I experiments.

Discussion

Photochemistry of Nitrogen. N_2 absorbs photons through slightly broadened partly overlapping rovibrational lines in the VUV region and dissociates via a repulsive triplet state (Fig. S1). Excitation of ground state N_2 molecules in the VUV yields several bound excited electronic singlet states with Σ and Π symmetries and, for each symmetry group, with two Rydberg and one valence state (25). As a consequence of interaction of Rydberg and valence states of both symmetries, perturbations are common (26–28). Spin-orbit coupling to triplet states, some of which are repulsive, leads to predissociation and accidental predissociation (29, 30). The extensive electronic state couplings result in a wide range of lifetimes for predissociation and are a strong function of isotope masses (30). A detailed quantum mechanical calculation (25) of the wavelength dependency for photoexcitation processes shows that ^{15}N enrichment can attain very high (>10,000‰) values and is highly sensitive to the excitation wavelength. It is suggested that the strongest isotope effect will occur in spectral regions where states of significantly different oscillator strengths are strongly mixed.

Isotopic Self-Shielding. The absorption of photons in a N_2 gas column is subject to shielding primarily by absorption of the more abundant $^{14}N_2$ isotopologue, resulting in an enrichment of ^{15}N in the dissociation product due to preferential absorption of the rarer $^{14}N^{15}N$ and $^{15}N^{15}N$ isotopologues (23). A rotationally resolved spectrum for each of the isotopomers was computed (Fig. S2) to model the N-isotopic fractionation for the experimental photolysis processes inside the reaction chamber, including temperature and pressure effects. Using this computed spectrum, the absorption of each isotopomer was calculated using the Beer−Lambert law, and the result was summed over the three isotopes to give the light intensity at the wavelength λ at a distance l along the length of the chamber. Since the radiative lifetimes for all states in the experimental wavelength range are much longer (on the order of nanoseconds) than the predissociation lifetimes (hundreds of picoseconds or less), we assumed the quantum yield of dissociation is unity. This means that

Table 1. Experimental conditions and isotope results from N_2 photolysis by VUV photons

Wavelength, nm	Time, min	N_2 yield, μmol	$\delta^{15}N_{AIR}$, ‰	BC-$\delta^{15}N_{AIR}$, ‰
Set-I (100 mtorr, −78 °C, column density = 5.2E17)				
80.7	468	1.28	2,432	2,451 ± 174
85.1	450	0.92	2,773	2,803 ± 199
86.7	470	0.09	2,386	2,690 ± 203
88.6	478	0.07	2,677	3,112 ± 241
90.0	416	0.03	6,397	10,149 ± 897
90.0	416	0.03	8,451	13,412 ± 1,185
92.0	460	0.14	2,682	2,887 ± 213
94.0	500	0.12	2,663	2,904 ± 215
96.1	416	0.07	1,058	1,229 ± 95
97.9	467	0.07	809	967 ± 73
Set-II (100 mtorr, 23 °C, column density = 3.43E17)				
88.6	300	0.10	1,611	1,796 ± 134
90.0	475	0.08	2,582	2,965 ± 225
91.5	483	0.12	2,130	2,332 ± 172
93.9	414	0.08	1,320	1,506 ± 115
97.3	422	0.07	555	648 ± 50
Set-III (62.5 mtorr, −78 °C, column density = 3.48E17)				
88.9	475	0.07	2,837	3,341 ± 256
90.0	420	0.05	2,909	3,566 ± 294
91.0	430	0.07	2,610	3,028 ± 235
Set-IV (100 mtorr, −15 °C, column density = 3.79E17)				
90.0	240	0.14	9,727	10,457 ± 770
Set-V (100 mtorr, −40 °C, column density = 3.86E17)				
90.0	450	0.08	8,560	9,874 ± 746

Blank experiments are performed, following all of the steps in the experiment excluding VUV photons. The measured values are corrected by isotope mass balance (see SI Materials and Methods for details), and the propagated errors are shown for the blank corrected (BC) values.
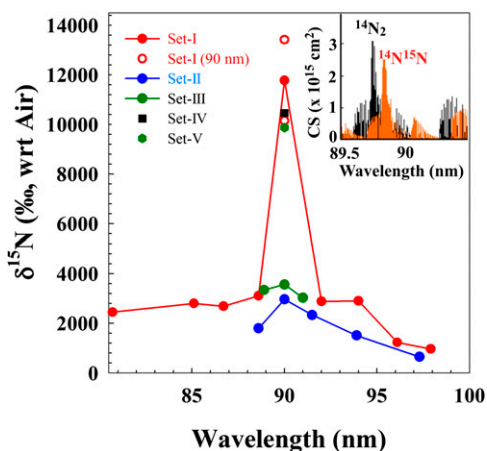
Fig. 2. The ^{15}N enrichment profile. Wavelength-dependent N-isotopic compositions with respect to (wrt) air composition in N_2 dissociation products by VUV photons in five different sets of experiments (mT refers to millitorr). The errors associated with the measurements are shown in Table 1 (typically are about three times of the size of the symbols). (*Inset*) The rovibrational spectra of $^{14}N_2$ and $^{14}N^{15}N$ with strong electronic state mixing around 90 nm, where massive N-isotopic fractionation was measured.

all excited states will eventually dissociate. The isotopic fractionation $\delta^{15}N$ was computed as a function of the central frequency of the ALS beam profile, for the entire wavelength range 80–98 nm (i.e., 100,000–120,000 cm^{-1}) and for different densities and temperatures. The details of the computational methodology are given in *SI Materials and Methods, Self-Shielding: Computational Methodology*.

Following the above methodology and using two different cross-section data sets from refs. 24 and 31, the wavelength-dependent enrichment profiles at different temperatures are computed as shown in Fig. 3, which shows higher enrichments compared with the experimentally measured (Fig. 2) values. The trend of the computed enrichment profiles with temperature and pressure variations qualitatively matches the experimental profile (Fig. S3). These computed profiles also show a significant dependence on column density, suggesting self-shielding is a contributor. However, the computed enrichment profile does not show the peak measured at 90 nm (Figs. 2 and 3).

The computed enrichment profiles (Fig. 3) show less shielding than is needed to account for the experimental results. The synchrotron beam profiles used in these experiments are about 2 nm wide (FWHM) (32) and, therefore, the measured enrichments are the average value over the wavelength region of the beam profile and may reflect lower limits. In the computation presented in Fig. 3, it is observed that if we sufficiently broaden the rotational bands to about 4 cm^{-1} (it is possible to change the line width for data set from ref. 24 following the computational steps mentioned in *SI Materials and Methods*), we reproduce the average experimentally measured enrichments (~2,200‰, excluding that measured at 90 nm) for the profile marked as "ML." One plausible physical explanation behind this discrepancy is that the mutual shielding may play a larger role than self-shielding at pressures used in these experiments. Although the overall enrichment profiles could be explained by self-shielding and mutual shielding, however, the measured enrichment peaks at around 90 nm in all of the five sets of experiments could not be explained by shielding consideration and may need additional mechanisms.

Perturbation-Governed Isotope Effects. The wavelength region of 90 nm stands out in electronic state mixing in the computed spectra as shown in Fig. S2. Huge isotopic enrichments are

measured for four sets (set-I, set-II, set-IV, and set-V) of experiments at around 90 nm compared with that measured in other spectral regions (Fig. 2) defining peaks in enrichment profiles. The notable feature is that the enrichment values for these four sets are inversely proportional to the photolysis temperatures, and no clear peak (considering errors) could be defined for set-III, which is performed at different column densities than those for the other sets. These features indicate the role of density of state variation in the state-mixing zone. It was shown previously that the perturbation in upper electronic states due to unusual state mixing gave rise to an unprecedented ^{15}N enrichment in the photodissociation process (25). While shielding-based computed enrichment profiles (Fig. 3) cannot explain the measured peaks in the enrichment profile at 90 nm, other perturbations and/or unrecognized sources are required to explain these observations. Therefore, extensive state mixing in localized regions of the spectrum (e.g., the b′–c′ mixing) may be one of the plausible reasons for the measured peak in enrichment profiles. In photodissociation, at the extreme of a quantum yield of one as assumed in the self-shielding computations, no isotope effect appears in the rate of N_2 predissociation. This assumption may not be correct for all of the absorption bands (33) and may affect the wavelength-dependent isotopic fractionation profile.

In summary, a wide range of ^{15}N enrichments were observed in the VUV spectral zone due to N_2 photodissociation, and part of these enrichments could be explained by self-shielding and mutual shielding. The shielding computation presented here assumes a quantum yield of unity for N_2 photodissociation, which may not be true for situations of extensive state mixing where perturbations play a significant role in determining the dissociation channels. These processes need to be considered, coupled with shielding, to fully explain the measured ^{15}N enrichments. It is not possible to identify the isotope effects due to shielding and due to perturbation separately from the measurements, and therefore, the measured ^{15}N enrichments are treated as an integrated "photochemical effect" in discussion of the implications of the measurements.

Implications

Nitrogen in Solar Nebula and IOM. The isotope inventory of nitrogen in astronomical environments is reasonably known. The solar system was formed with an initial $^{15}N/^{14}N$ ratio acquired from parental molecular clouds from interstellar medium (ISM).

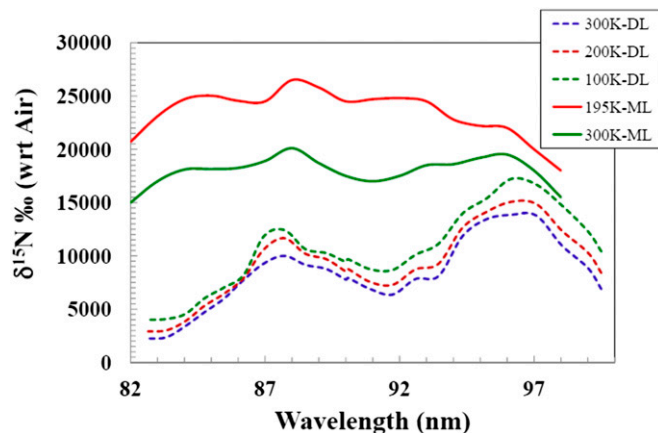**Fig. 3.** Self-shielding based computed enrichment profiles of ^{15}N using photodissociation cross-section data from refs. 24 and 31 simulating the experimental conditions at different temperatures. "ML" and "DL" refer to the cross-section data from refs. 24 and 31, respectively. Neither of these simulated enrichment profiles depicts the enrichment feature (peak at around 90 nm) as measured in the experiments.
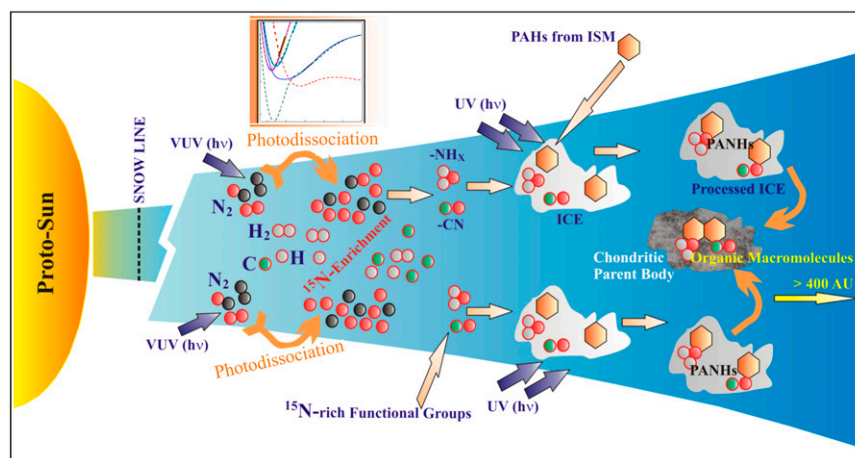
Chakraborty et al.

Fig. 4. Schematic diagram of the solar nebula. Synthesis of ^{15}N-rich PANHs inside the ice is possible, while PAHs and ^{15}N-rich nitrile and amine functional groups are frozen in ice and exposed to UV photons. The source of ^{15}N enrichment is the VUV photodissociation as shown in the present study. PANHs are incorporated in the chondritic parent bodies as organic macromolecules at a later stage.

The near-identical ratios measured in solar wind and the Jovian atmosphere may indicate the formation of the gas giant with the initial solar system materials having the same N-isotopic composition, e.g., the bulk nebular nitrogen isotopic ratio is represented by the Sun and Jupiter, while the terrestrial ratio represents considerable processing from the original starting values and meteoritic materials represent various intermediate or more extreme values as depicted in Fig. 1.

The organic material in carbonaceous chondrites hosts the enriched ^{15}N components (Fig. 1B), mostly as IOM. These macromolecular materials encompass condensed aromatics at their cores, connected by aliphatic and ether linkages and with various functional groups (e.g., nitrile, amine etc) attached, and are suggested to be of common origin (34). Aromatic molecules (polycyclic aromatic hydrocarbons, PAHs) are ubiquitous in the ISM and are the most common class of organic compounds in the universe in gas phase as well as in carbonaceous dust (35, 36). When nitrogen replaces a carbon in the ring structure, it forms polycyclic aromatic nitrogen heterocycles (PANHs). Nucleobases, the essential building block for the origin of life, are PANHs and are a prebiotically significant component (36). It is possible that PANHs are formed inside the solar system by nitrogenation of PAHs. Laboratory experiments depict nitrogenation of PAHs to form PANHs while frozen in ice along with nitrile and amine functional groups and exposed to UV radiation (37). The initiating step in these processes would be the production of a highly enriched ^{15}N atom from N_2 photodissociation (the integrated photochemical effect) as demonstrated in the present experiment at the outer edges of the disk where VUV was not opaque. This process may potentially generate ^{15}N-enriched amine and nitrile group molecules from a ^{15}N-rich atomic nitrogen pool. The present experimental study suggests that formation of nitrile functional groups through gas-phase reactions following N_2 photodissociation is plausible (38). Once formed, these functional groups may freeze-out in the ice and possibly synthesize PANHs with high ^{15}N enrichment under UV exposure within the ice (37, 39–41) (Fig. 4). The ^{15}N enrichments measured in meteorite organics perhaps originated through this pathway, and this proposition would not simultaneously enrich D and ^{15}N as observed in many cases (18).

Accommodation of Entire N-Isotopic Range Through Photodissociation.
The range in observed nitrogen isotopic compositions extends to ~4,000‰ (Fig. 1); thus an isotope altering process of this magnitude is needed to account for the observations. The

present experiments show that at selected wavelengths, nitrogen photolytic effects of more than double this range (11,780‰, average of two separate experiments, Fig. 2 and Table 1) are observed. Without the spectacular enrichment at 90 nm, a (self- and mutual) shielding-dominated isotopic enrichment would yield an average value of about 2,200‰ (Table 1), which is less than that measured in some IOMs. The interstellar radiation field and the solar spectrum are considered to be wavelength dependent (42, 43). Coupling of a wavelength-dependent massive isotope effect with a wavelength-variable VUV field may result in occasional high enrichments. Fig. 5 schematically shows the structured solar VUV field (43) together with the measured wavelength-dependent enrichment profile, depicting a possibility of variable enrichment profile across the wavelength in the solar nebula. A huge enrichment may result due to the combined enhancement of both the factors in localized spectral region such as that at 90 nm. Therefore, occasionally high ^{15}N isotopic enrichment is not unusual for such smaller random samples (such as that of IOMs) and, that deviate considerably from the average. Such effects could explain the entire range of meteoritic measurements, although full photochemical modeling would be necessary. There may be other processes (e.g., Haber−Bosch-type reactions of N_2 and H_2 on grain surface) that may form nitrile and amine functional group without any ^{15}N enrichment and that
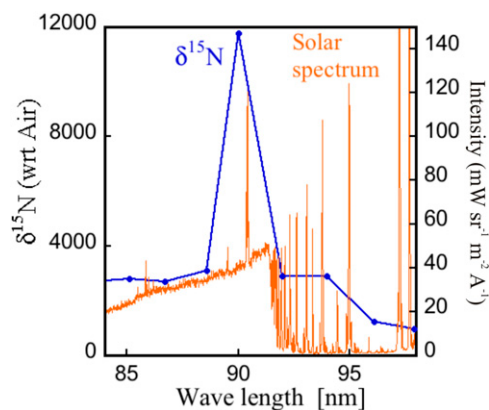

Fig. 5. Measured ^{15}N fractionation superimposed with solar spectrum. Shown is the measured fractionation as a function of wavelength, and the intensity distribution (ordinate on the right) of the solar spectrum (43).

would dilute the photochemically enriched ^{15}N signature and should be incorporated into the full model. It is also clear that in any consideration, the next generation of models must include both the isotope effect of the nitrogen molecule and self-shielding so that the precise fractional contributions may be determined. The present work lays the foundation of the fundamental process for the first time, to our knowledge, and allows this next step to be taken in a direct way.

Conclusions

Nitrogen isotopic distribution among the solar system materials varies in a wide range. The largest enrichments in heavy isotope of nitrogen reside in organic materials, which are presumably formed at the cold icy regions of the nebula. The enrichments in heavy nitrogen isotopes are not always accompanied by the heavy isotopes of carbon or hydrogen. The leading ion−molecular exchange hypothesis in the dense cold cloud predicts simultaneous enrichment of the heavy isotope of these elements, contrary to observations. The N-isotopic fraction during VUV photodissociation is presented here and exhibits an unprecedented isotopic enrichment at specific wavelengths, arising due to the predissociative nature of dissociation via complex multiple (excited) state mixing. It is highly plausible that the entire meteoritic N-isotope range can be accommodated simply by the photochemical effect (including self-shielding and mutual shielding and perturbations) during photodissociation of N_2. The bulk nebular N-isotopic ratio is represented by the Sun and Jupiter, while the terrestrial ratio and the ratios from the meteoritic materials represent considerable processing from the original starting values, and the bulk of the processing must have occurred in the solar nebula.

Materials and Methods

Gas mixtures of N_2 and H_2 were photolyzed using VUV photons from the ALS synchrotron at nine different wavelength bands (of FWHM of ~2 nm) between 80 nm and 98 nm in a differentially pumped reaction chamber (Fig. S4) described earlier (44). In five different sets, 20 individual photolysis experiments were performed, each with duration of 4–8 h and varying pressure of the gas mixture and temperature of the reaction chamber. The trapping of the N_2 photodissociation product, N atoms, is nontrivial. A steady flow of high-purity premix gas (N_2:H_2 = 50:50) was established in the precooled (−78 °C) reaction chamber at a total pressure of 200 mtorr (column density ~4 × 10^{17} molecules per square centimeter) for set-I experiments. In this set, photolysis of this gas mixture was carried out at nine different synchrotron bands (FWHM = 2.2 nm) within the range of 80–98 nm separately in nine different experiments. Set-II experiments were performed with the same pressure as that of set-I (N_2 partial pressure, P_{N2} = 100 mtorr), but at 23 °C temperature. Set-III experiments were performed with of P_{N2} of 62 mtorr, but at the same temperature (−78 °C) as that of set-I. Set-IV and set-V experiments were performed at P_{N2} = 100 mtorr, and at two intermediate temperatures, i.e., −15 °C and −40 °C, respectively. For all of the five sets of experiments, photolytically produced atomic N was cryogenically trapped by liquid nitrogen as NH_3 and collected in sample tubes and returned to University of California, San Diego, for analysis. The NH_3 yield was low and based on absorption cross sections, varying between 0.1 micromoles and 1.3 micromoles. N_2 was produced by pyrolyis (in presence of CuO) of NH_3 as described by ref. 45. Finally, N-isotopic composition of N_2 was measured using a Finnigan MAT 253 isotope-ratio mass spectrometer.

1. Thiemens MH, Chakraborty S, Dominguez G (2012) The physical chemistry of mass-independent isotope effects and their observation in nature. *Annu Rev Phys Chem* 63(1):155–177.
2. Marty B, Chaussidon M, Wiens RC, Jurewicz AJG, Burnett DS (2011) A ^{15}N-poor isotopic composition for the solar system as shown by Genesis solar wind samples. *Science* 332(6037):1533–1536.
3. Abbas MM, et al. (2004) The nitrogen isotopic ratio in Jupiter's atmosphere from observations by the Composite Infrared Spectrometer on the Cassini spacecraft. *Astrophys J* 602(2):1063.
4. Busemann H, et al. (2006) Interstellar chemistry recorded in organic matter from primitive meteorites. *Science* 312(5774):727–730.
5. Briani G, et al. (2009) Pristine extraterrestrial material with unprecedented nitrogen isotopic variation. *Proc Natl Acad Sci USA* 106(26):10522–10527.
6. Kerridge JF (1985) Carbon, hydrogen and nitrogen in carbonaceous chondrites: Abundances and isotopic compositions in bulk samples. *Geochim Cosmochim Acta* 49(8):1707–1714.
7. Kung C-C, Clayton RN (1978) Nitrogen abundances and isotopic compositions in stony meteorites. *Earth Planet Sci Lett* 38(2):421–435.
8. Grady MM, Wright IP, Carr LP, Pillinger CT (1986) Compositional differences in enstatite chondrites based on carbon and nitrogen stable isotope measurements. *Geochim Cosmochim Acta* 50(12):2799–2813.
9. Robert F, Epstein S (1982) The concentration and isotopic composition of hydrogen, carbon and nitrogen in carbonaceous meteorites. *Geochim Cosmochim Acta* 46(1):81–95.
10. Ivanova MA, et al. (2008) The Isheyevo meteorite: Mineralogy, petrology, bulk chemistry, oxygen, nitrogen, carbon isotopic compositions, and ^{40}Ar-^{39}Ar ages. *Meteorit Planet Sci* 43(5):915–940.
11. Prombo CA, Clayton RN (1985) A striking nitrogen isotope anomaly in the Bencubbin and Weatherford meteorites. *Science* 230(4728):935–937.
12. Prombo CA, Clayton RN (1993) Nitrogen isotopic compositions of iron meteorites. *Geochim Cosmochim Acta* 57(15):3749–3761.
13. McKeegan KD, et al. (2006) Isotopic compositions of cometary matter returned by Stardust. *Science* 314(5806):1724–1728.
14. Bockelée-Morvan D, et al. (2008) Large excess of heavy nitrogen in both hydrogen cyanide and cyanogen from Comet 17P/Holmes. *Astrophys J Lett* 679(1):L49.
15. Floss C, et al. (2004) Carbon and nitrogen isotopic anomalies in an anhydrous interplanetary dust particle. *Science* 303(5662):1355–1358.
16. Alexander CMOD, et al. (1998) The origin of chondritic macromolecular organic matter: A carbon and nitrogen isotope study. *Meteorit Planet Sci* 33(4):603–622.
17. Engel MH, Macko SA (2001) The stereochemistry of amino acids in the Murchison meteorite. *Precambrian Res* 106(1-2):35–45.
18. Jérôme A (2010) Multiple origins of nitrogen isotopic anomalies in meteorites and comets. *Astrophys J* 722(2):1342.
19. Millar TJ, Roberts H, Markwick AJ, Charnley SB (2000) The role of H_2D^+ in the deuteration of interstellar molecules. *Philos Trans R Soc A* 358(1774):2535–2547.
20. Rodgers SD, Charnley SB (2008) Nitrogen superfractionation in dense cloud cores. *Mon Not R Astron Soc Lett* 385(1):L48–L52.
21. Rodgers SD, Charnley SB (2008) Nitrogen isotopic fractionation of interstellar nitriles. *Astrophys J* 689(2):1448.
22. Eva SW, Steven BC, Martin AC, Stefanie NM (2012) Isotopic anomalies in primitive solar system matter: Spin-state-dependent fractionation of nitrogen and deuterium in interstellar clouds. *Astrophys J Lett* 757(1):L11.
23. Clayton RN (2002) Solar system: Self-shielding in the solar nebula. *Nature* 415(6874):860–861.
24. Muskatel BH, Remacle F, Levine RD (2012) Ultrafast predissociation mechanism of the $^1\Pi_u$ states of $^{14}N_2$ and its isotopomers upon attosecond excitation from the ground state. *J Phys Chem A* 116(46):11311–11318.
25. Muskatel BH, Remacle F, Thiemens MH, Levine RD (2011) On the strong and selective isotope effect in the UV excitation of N_2 with implications toward the nebula and Martian atmosphere. *Proc Natl Acad Sci USA* 108(15):6020–6025.
26. Huber KP, Chan M-C, Stark G, Ito K, Matsui T (2009) N_2 band oscillator strengths at near-threshold energies. *J Chem Phys* 131(8):084301.
27. Lefebvre-Brion H, Lewis BR (2007) Comparison between predissociation mechanisms in two isoelectronic molecules: CO and N_2. *Mol Phys* 105(11-12):1625–1630.
28. Baker J, Launay F (2005) Identification and analysis of the perturbed $c^3\Pi$ (ν = 1) − $X^1\Sigma^+$ and $k^3\Pi$ (ν = 5) − $X^1\Sigma^+$ absorption bands of carbon monoxide. *J Chem Phys* 123(23):234302.
29. Lefebvre-Brion H, Field RW (2004) *The Spectra and Dynamics of Diatomic Molecules* (Elsevier, New York), 2nd Ed.
30. Lewis BR, Gibson ST, Zhang W, Lefebvre-Brion H, Robbe J-M (2005) Predissociation mechanism for the lowest $^1\Pi_u$ states of N_2. *J Chem Phys* 122(14):144302.
31. Liang M-C, Heays AN, Lewis BR, Gibson ST, Yung YL (2007) Source of nitrogen isotope anomaly in HCN in the atmosphere of Titan. *Astrophys J Lett* 664(2):L115.
32. Chakraborty S, Ahmed M, Jackson TL, Thiemens MH (2009) Response to comments on "Experimental test of self-shielding in vacuum ultraviolet photodissociation of CO." *Science* 324(5934):1516.
33. Lewis BR, Heays AN, Gibson ST, Lefebvre-Brion H, Lefebvre R (2008) A coupled-channel model of the $^3\Pi_u$ states of N_2: Structure and interactions of the $3s\sigma_gF_3{}^3\Pi_u$ and $3p\pi_uG_3{}^3\Pi_u$ Rydberg states. *J Chem Phys* 129(16):164306.
34. Sephton MA, Gilmour I (2000) Aromatic moieties in meteorites: Relics of interstellar grain processes? *Astrophys J* 540(1):588–591.
35. Bernstein MP, Mattioda AL, Sandford SA, Hudgins DM (2005) Laboratory infrared spectra of polycyclic aromatic nitrogen heterocycles: Quinoline and phenanthridine in solid argon and H_2O. *Astrophys J* 626(2):909.
36. Peeters Z, Botta O, Charnley SB, Ruiterkamp R, Ehrenfreund P (2003) The astrobiology of nucleobases. *Astrophys J Lett* 593(2):L129.

37. Bernstein MP, et al. (2003) Side group addition to the polycyclic aromatic hydrocarbon coronene by ultraviolet photolysis in cosmic ice analogs. *Astrophys J* 582(1):L25.
38. Imanaka H, Smith MA (2010) Formation of nitrogenated organic aerosols in the Titan upper atmosphere. *Proc Natl Acad Sci USA* 107(28):12423–12428.
39. Bernstein MP, et al. (1999) UV irradiation of polycyclic aromatic hydrocarbons in ices: Production of alcohols, quinones, and ethers. *Science* 283(5405):1135–1138.
40. Yabushita A, Hama T, Kawasaki M (2013) Photochemical reaction processes during vacuum-ultraviolet irradiation of water ice. *J Photochem Photobiol Photochem Rev* 16(0):46–61.
41. Murthy SG, Rui Y (2012) In-situ probing of radiation-induced processing of organics in astrophysical ice analogs—Novel laser desorption laser ionization time-of-flight mass spectroscopic studies. *Astrophys J Lett* 756(1):L24.
42. Draine BT (1978) Photoelectric heating of interstellar gas. *Astrophys J Suppl* 36:595–619.
43. Curdt W, et al. (2001) The SUMER spectral atlas of solar-disk features. *Astron Astrophys* 375(2):591–613.
44. Chakraborty S, Ahmed M, Jackson TL, Thiemens MH (2008) Experimental test of self-shielding in vacuum ultraviolet photodissociation of CO. *Science* 321(5894):1328–1331.
45. Li L, Cartigny P, Ader M (2009) Kinetic nitrogen isotope fractionation associated with thermal decomposition of NH_3: Experimental results and potential applications to trace the origin of N_2 in natural gas and hydrothermal systems. *Geochim Cosmochim Acta* 73(20):6282–6297.
46. Rai VK, Murty SVS, Ott U (2003) Nitrogen components in ureilites. *Geochim Cosmochim Acta* 67(12):2213–2237.
47. Owen T, Mahaffy PR, Niemann HB, Atreya S, Wong M (2001) Protosolar nitrogen. *Astrophys J* 553:L77–L79.
48. Kerridge JF (1993) Long-term compositional variation in solar corpuscular radiation: Evidence from nitrogen isotopes in the lunar regolith. *Rev Geophys* 31(4):423–437.
49. Huss GR, Nagashima K, Jurewicz AJG, Burnett DS, Olinger CT (2012) The isotopic composition and fluence of solar-wind nitrogen in a genesis B/C array collector. *Meteorit Planet Sci* 47(9):1436–1448.
50. Mohapatra RK, Murty SVS (2003) Precursors of Mars: Constraints from nitrogen and oxygen isotopic compositions of martian meteorites. *Meteorit Planet Sci* 38(2):225–241.

EARTH, ATMOSPHERIC, AND PLANETARY SCIENCES